

The Coupling Cloud: A community database of megathrust kinematic coupling models

Bar Oryan ¹, Alice-Agnes Gabriel ^{1,2}, Roland Bürgmann ³, Eric Calais ⁴, Guo Cheng ⁵, Mohamed Chlieh ⁶, Beatriz Cosenza-Murales ⁷, Víctor M. Cruz-Atienza ⁸, Luca Dal Zilio ^{9,10}, Charles DeMets ¹¹, Andria Ellis ¹², Lujia Feng ^{9,10}, Jeffrey T. Freymueller ¹³, Endra Gunawan ¹⁴, Nuraini R. Hanifa ¹⁵, George E. Hilley ¹⁶, Ya-Ju Hsu ¹⁷, Takeshi Iinuma ¹⁸, Yuji Itoh ¹⁹, Jorge Jara ²⁰, Kaj M. Johnson ²¹, Romain Jolivet ^{4,22}, Masayuki Kano ²³, Emilie Klein ⁴, Shanshan Li ²⁴, Shaoyang Li ²⁵, Eric O. Lindsey ²⁶, Zhen Liu ²⁷, John P. Loveless ²⁸, Bertrand Loverly ⁶, Louise Maubant ¹⁹, Sylvain Michel ^{29,30}, Cyril Muller ³¹, Marianne Métois ³², Takuya Nishimura ²³, Akemi Noda ^{19,33}, Dibyashakti Panda ³⁴, Mason Perry ⁹, Raymundo Plata-Martinez ³⁵, Mathilde Radiguet ⁶, Baptiste Rousset ³⁵, Elizabeth M. Sherrill ³⁶, Anne Socquet ⁶, Juan Carlos Villegas-Lanza ³⁷, Laura M. Wallace ^{36,38}, Lian Xue ³⁹, Yusuke Yokota ⁴⁰, Shoichi Yoshioka ^{41,42}, Shui-Beih Yu ¹⁷

¹Scripps Institution of Oceanography, University of California at San Diego, La Jolla, CA 92093, USA, ²Department of Earth and Environmental Sciences, Ludwig-Maximilians-University, 80333 Munich, Germany, ³Department of Earth and Planetary Science, UC Berkeley, ⁴Laboratoire de Géologie, Ecole normale supérieure - PSL, CNRS UMR 8538, Paris France, ⁵Nevada Bureau of Mines and Geology, University of Nevada, Reno, NV, USA, ⁶Univ. Grenoble Alpes, Univ. Savoie Mont Blanc, CNRS, IRD, Univ. Gustave Eiffel, STerre, 38000 Grenoble, France, ⁷Instituto de Investigación en Ciencias Físicas y Matemáticas (IFIM), Escuela de Ciencias Físicas y Matemáticas, Universidad de San Carlos de Guatemala, ⁸Instituto de Geofísica, Universidad Nacional Autónoma de México, ⁹Earth Observatory of Singapore, Nanyang Technological University, Singapore, Singapore, ¹⁰Asian School of the Environment, Nanyang Technological University, Singapore, Singapore, ¹¹Department of Geoscience, University of Wisconsin-Madison, Madison WI 53706 USA, ¹²U.S. Geological Survey, Hawaiian Volcano Observatory, Hilo, Hawaii, USA, ¹³Department of Earth and Environmental Sciences, Michigan State University, East Lansing, MI, USA, ¹⁴Institut Teknologi Bandung, Indonesia, ¹⁵Research Center for Geological Disaster, National Research and Innovation Agency, Bandung, Indonesia, ¹⁶Stanford University, Stanford, CA, USA, ¹⁷Institute of Earth Sciences, Academia Sinica, ¹⁸Japan Agency for Marine-Earth Science and Technology, Yokohama, Japan, ¹⁹Earthquake Research Institute, The University of Tokyo, Tokyo, Japan, ²⁰GFZ Helmholtz Centre for Geosciences, Potsdam, Germany, ²¹Department of Earth and Atmospheric Sciences, Indiana University, Bloomington, IN, USA, ²²Institut Universitaire de France, 1 rue Descartes, 75006 Paris, France, ²³Disaster Prevention Research Institute, Kyoto University, Japan, ²⁴School of Computing at University of Wyoming, ²⁵State Key Laboratory of Lithospheric and Environmental Coevolution, Institute of Geology and Geophysics, Chinese Academy of Sciences, Beijing, China, ²⁶Department of Earth & Planetary Sciences, University of New Mexico, Albuquerque, NM, USA, ²⁷Jet Propulsion Laboratory, California Institute of Technology, ²⁸Department of Geosciences, Smith College, Northampton, MA, USA, ²⁹Université Côte d'Azur, IRD, CNRS, Observatoire de la Côte d'Azur, Valbonne, France, ³⁰Sorbonne Université, CNRS-INSU, Institut des Sciences de la Terre Paris, IStEP UMR 7193, Paris, France, ³¹Observatorio Vulcanológico y Sismológico de Costa Rica, Universidad Nacional de Costa Rica Heredia, Costa Rica, ³²Université Claude Bernard Lyon 1, ENS de Lyon, Université Jean Monnet, CNRS, LGL-TPE, UMR5276, ³³Meteorological Research Institute, Tsukuba, Japan, ³⁴Department of Geology, School of Earth Sciences, Central University of Tamil Nadu, Thiruvavur, India, 610005, ³⁵Institut Terre et Environnement de Strasbourg UMR7063, Université de Strasbourg/CNRS/ENGESS, 5 Rue René Descartes, Strasbourg, 67000, France, ³⁶GEOMAR Helmholtz Centre for Ocean Research Kiel, Germany, ³⁷Instituto Geofísico del Perú (IGP), Lima, Peru, ³⁸Institute for Geophysics, University of Texas, Austin, TX, USA, ³⁹School of Earth and Space Science, Peking University, Beijing, China, ⁴⁰Institute of Industrial Science, University of Tokyo, Japan, ⁴¹Research Center for Urban Safety and Security, Kobe University, Rokkodai-cho 1-1, Nada ward, Kobe 657-8501, Japan, ⁴²Department of Planetology, Graduate School of Science, Kobe University, Rokkodai-cho 1-1, Nada ward, Kobe 657-8501, Japan

Author contributions: *Conceptualization:* B. Oryan, A. Gabriel. *Data Curation:* B. Oryan, A. Gabriel, R. Bürgmann, E. Calais, G. Cheng, M. Chlieh, B. Cosenza-Murales, V. Cruz-Atienza, L. Dal Zilio, C. DeMets, A. Ellis, L. Feng, J. Freymueller, E. Gunawan, N. Hanifa, G. Hilley, Y. Hsu, T. Iinuma, Y. Itoh, J. Jara, K. Johnson, R. Jolivet, M. Kano, E. Klein, S. Li, S. Li, E. Lindsey, Z. Liu, J. Loveless, B. Loverly, L. Maubant, S. Michel, C. Muller, M. Métois, T. Nishimura, A. Noda, D. Panda, M. Perry, R. Plata-Martinez, M. Radiguet, B. Rousset, E. Sherrill, A. Socquet, J. Villegas-Lanza, L. Wallace, L. Xue, Y. Yokota, S. Yoshioka, S. Yu. *Validation:* B. Oryan, A. Gabriel, R. Bürgmann, E. Calais, G. Cheng, M. Chlieh, B. Cosenza-Murales, V. Cruz-Atienza, L. Dal Zilio, C. DeMets, A. Ellis, L. Feng, J. Freymueller, E. Gunawan, N. Hanifa, G. Hilley, Y. Hsu, T. Iinuma, Y. Itoh, J. Jara, K. Johnson, R. Jolivet, M. Kano, E. Klein, S. Li, S. Li, E. Lindsey, Z. Liu, J. Loveless, B. Loverly, L. Maubant, S. Michel, C. Muller, M. Métois, T. Nishimura, A. Noda, D. Panda, M. Perry, R. Plata-Martinez, M. Radiguet, B. Rousset, E. Sherrill, A. Socquet, J. Villegas-Lanza, L. Wallace, L. Xue, Y. Yokota, S. Yoshioka, S. Yu. *Funding Acquisition:* B. Oryan, A. Gabriel. *Methodology:* B. Oryan, A. Gabriel. *Project Administration:* B. Oryan, A. Gabriel. *Software:* B. Oryan. *Supervision:* A. Gabriel. *Visualization:* B. Oryan. *Writing – original draft:* B. Oryan, A. Gabriel. *Writing – review & editing:* B. Loverly, C. Muller, R. Bürgmann, E. Calais, J. Freymueller, M. Métois, V. Cruz-Atienza, T. Nishimura, E. Klein, C. DeMets, D. Panda, L. Maubant, S. Yoshioka, J. Jara, M. Radiguet, S. Michel, Y. Hsu, Y. Itoh, L. Feng, S. Li, R. Jolivet, J. Loveless, J. Villegas-Lanza, Y. Yokota, M. Perry, B. Rousset, Z. Liu, B. Cosenza-Murales, R. Plata-Martinez, N.R. Hanifa, E. Lindsey, E. Sherrill.

Production Editor:
Andrea Llenos
Handling Editor:
Wenbin Xu
Copy & Layout Editor:
Miguel Neves

Received:
January 31, 2026
Accepted:
April 13, 2026
Published:
May 19, 2026

Abstract Kinematic coupling models inverted from geodetic data are widely used to evaluate how slip deficit is distributed along subduction megathrusts during the interseismic period, and are central to earthquake and tsunami hazard assessment. Yet, existing coupling models differ widely in methodology and inputs, lack common community standards, and are scattered across publications and repositories. Here, we introduce the “Coupling Cloud” (<https://couplingcloud.ucsd.edu>), an open, extensible, community-driven platform that curates, standardizes, documents, and disseminates more than 96 kinematic coupling models from 55 publications across 21 subduction margins. The platform provides interactive 2D and 3D plate-interface viewers to inspect coupling models together with associated information such as slab geometry, uncertainty estimates and metadata. All datasets can be downloaded directly in standardized formats: surface-projected coupling values as NetCDF, plate-interface dislocation geometries as VTU, and model metadata as YAML files. We demonstrate the advantages of centralized and standardized coupling data through a Cascadia subduction zone example, where synthesizing eight full-margin models reveals along-strike patterns that are not apparent when models are examined individually. Consolidating coupling models within a coherent, version-controlled framework enables systematic cross-margin comparison and FAIR-compliant data sharing, opening the door to more comprehensive assessment of megathrust mechanics.

1 Introduction

Community databases can accelerate Earth science research by standardizing how data products are archived and shared, enabling synthesis across models and systematic evaluation of methodological choices. Several initiatives illustrate the scientific value of open, standardized data infrastructures. For example, SubMachine compiles global seismic tomography models (Hosseini et al., 2018), the SubMap initiative assembles long-term subduction zone observations (<https://submap.gm.umontpellier.fr/>), and the Nevada Geodetic Laboratory provides processed GNSS time series and velocity fields (Blewitt et al., 2018). Similarly, the SRC-MOD database unified finite-fault source inversion formats and metadata to aggregate hundreds of finite slip models (Mai and Thingbaijam, 2014), directly motivating community benchmarks such as the Source Inversion Validation exercises (SIV, Mai et al., 2016a). The USGS finite-fault model archive provides another example of how openly accessible, consistently formatted datasets accelerate scientific discovery (Goldberg et al., 2022; Hayes, 2017). In contrast, despite the central role of coupling models in subduction zone science and hazard assessment, the geodetic megathrust coupling community has lacked a centralized, standardized infrastructure for archiving, comparing, and reusing published models in consistent, interoperable data formats.

Kinematic coupling models identify regions along subduction interfaces that accommodate little interseismic slip, commonly inferred as frictionally locked, amid regions that creep steadily or slip transiently during the interseismic period. These models are constructed from inversions of interseismic or inter-slow slip events (inter-SSE) surface displacements most commonly derived from GNSS (Dixon, 1991; Feigl et al., 1993) and InSAR (Bürgmann et al., 2000), but also incorporating leveling (Burgette et al., 2009; Jackson and Bilham, 1994), coral-based reconstructions (Chlieh et al., 2008; Tsang et al., 2015) and offshore geodetic measurements such as GNSS-Acoustic techniques (DeSanto et al., 2025; Gagnon et al., 2005; Yokota et al.,

2016). Such inversions commonly use Green’s functions from forward models based on elastic dislocation theory in a half-space (Meade, 2007; Okada, 1986, 1992), or viscoelastic earthquake-cycle formulations (Itoh et al., 2021; Li et al., 2015, 2018; Pollitz, 1997) and the backslip formulation to infer slip deficit (Savage, 1983). The inverse problem is then solved with linear schemes (Tarantola, 2005; Tarantola and Valette, 1982) or Bayesian approaches that integrate priors with data to quantify posterior uncertainty (e.g., Fukuda and Johnson, 2008; Minson et al., 2013; Tomita et al., 2021; Yabuki and Matsu’ura, 1992). Expressing the inferred slip deficit rate relative to the long-term plate convergence rate yields a kinematic coupling model (Wang and Dixon, 2004) that describes a continuous spectrum of fault behavior, ranging from areas creeping at the long-term slip rate (coupling ≈ 0) to effectively fixed regions with no creep (coupling ≈ 1).

Because kinematic coupling models delineate regions where elastic strain accumulates and may be released in future megathrust earthquakes, they are an important tool for assessing seismic and tsunami hazard in subduction zones (e.g., Giardini et al., 1999; Glehman et al., 2025; Ramos et al., 2021; Widiyantoro et al., 2020; Small and Melgar, 2021; Wang et al., 2015; Wang, 2010). However, despite their scientific value, these models face methodological challenges. Differences in assumed slab geometry and viscoelastic earth structure (Laske et al., 2013; Loverly et al., 2025; Luo et al., 2025; Wang et al., 2021), the period studied, density and quality of geodetic observations, velocity plate model, and the imposed regularization applied during coupling inversion affect the resulting coupling distributions (Fukuda and Johnson, 2008; Ide, 2007; Minson et al., 2013). Moreover, kinematic coupling models have traditionally lacked a unified, FAIR-compliant (Findable, Accessible, Interoperable, Reusable; Wilkinson et al., 2016) data format and are often scattered across publications in forms that are difficult to extract, evaluate, or systematically compare, limiting reproducibility and efforts to assess how modeling assumptions affect coupling estimates.

Here, we present the Coupling Cloud (<https://couplingcloud.ucsd.edu>, hereafter abbreviated to CC), an open online platform that aggregates a growing collection of published kinematic coupling models from subduction zones worldwide. The CC provides an intuitive interface to explore, visualize, and download

*Corresponding author: bar.oryan@columbia.edu

†Now at National Institute of Advanced Industrial Science and Technology, Tsukuba, Japan

these version controlled models, featuring a 2D map viewer for surface-projected coupling values and a 3D viewer that displays coupling on the underlying slab geometry. By centralizing and unifying these datasets and providing both 2D and 3D visualization tools within a single platform, the CC facilitates comparative analysis, strengthens reproducibility, and broadens community access to essential megathrust earthquake science resources. We demonstrate the value of this unified framework with a Cascadia case study, where along-strike patterns emerging from averaged models are not apparent when models are examined individually.

2 Data selection

As of January 12, 2026 the CC database comprises 96 kinematic coupling datasets compiled from 55 publications covering 21 subduction zones worldwide, for a total of 219 spatial data products. These represent all published coupling models for which datasets were available and that use geodetic observations to infer the spatial distribution of coupling along subduction megathrusts. The database currently includes (in alphabetical order) two models in Alaska and the Aleutians (Drooff and Freymueller, 2021; Li and Freymueller, 2018), two in the Caribbean (van Rijsingen et al., 2020), eleven in Cascadia (Li et al., 2018; Lindsey et al., 2021; Materna et al., 2023; Michel et al., 2018; Pollitz and Evans, 2017; Pollitz, 2025; Schmalzle et al., 2014; Sherrill et al., 2024), eight in Chile (Jara et al., 2024; Jolivet et al., 2020; Klein et al., 2018; Li et al., 2015; Métois et al., 2012, 2013, 2016), four in Costa Rica (Feng et al., 2012; Perry et al., 2025; Xue et al., 2015), two in Ecuador-Colombia (Chlieh et al., 2021; Gombert et al., 2018), one in Guatemala (Ellis et al., 2019), six in Hikurangi (Maubant et al., 2023; Michel et al., 2025; Wallace et al., 2012), three in Himalayas (Dal Zilio et al., 2020; Panda and Lindsey, 2024; Stevens and Avouac, 2015), one in Indo-Burma (Lindsey et al., 2023), nineteen in the Japan Trench (Abe and Yoshioka, 2022; Itoh et al., 2021; Lindsey et al., 2021; Loveless and Meade, 2016), two in Java (Hanifa et al., 2014; Widiyantoro et al., 2020), four in Kamchatka (Bürgmann et al., 2005), two in Manila (Hsu et al., 2016), two in Makran (Cheng et al., 2024), six in Mexico (Cosenza-Muralles et al., 2021; Cruz-Atienza et al., 2025; Maubant et al., 2022; Radiguet et al., 2016; Rousset et al., 2015), nine in Nankai (Liu et al., 2010; Loveless and Meade, 2016; Nishimura et al., 2018; Noda et al., 2018; Plata-Martinez et al., 2024; Sherrill et al., 2024; Yokota et al., 2016), ten in Peru (Jara et al., 2024; Lovery et al., 2024; Villegas-Lanza et al., 2016), one in Ryukyu (Kano et al., 2021), three in the Sagami trough (Loveless and Meade, 2016; Nishimura et al., 2018), and one in Sumatra (Chlieh et al., 2008). While the Coupling Cloud provides standardized access to these datasets, users are expected to cite the original publications associated with each model when using the data.

3 Data standardization and unified representation

Published coupling models vary widely in format and metadata, reflecting the diversity of data coverage, methods, and conventions used across studies and time. To standardize access and promote FAIR use (Wilkinson et al., 2016), we map each model onto a uniform latitude–longitude grid and store it as a NetCDF file (Rew and Davis, 1990). When gridded outputs are not provided, coupling fields are interpolated onto a regular grid with adaptively refined resolution using linear or triangular interpolation (Text S1, Fig. S1). Every file contains latitude, longitude, the coupling values, and additional optional parameters, such as standard deviation, interface depth, and slip deficit. The NetCDF format is machine-readable and supports direct analyses and visualization using open-source packages such as Matplotlib (Hunter, 2007), GMT (Wessel et al., 2019), and Xarray (Hoyer and Hamman, 2017). Because NetCDF files do not inherently preserve the original fault-dislocation geometry used to invert the geodetic observations, we reformat all available model dislocation geometries as VTU PolyData files (Schroeder et al., 1998). VTU is a widely adopted, self-describing format for unstructured meshes that natively supports complex 3D slab geometries and mixed element types, making it well suited for downstream use in numerical modeling workflows. This standardized format allows for direct visualization and processing using open-source tools such as ParaView (Ahrens et al., 2005), PyVista (Sullivan and Kaszynski, 2019), and Meshio (Schlömer, 2022) and preserves node coordinates, mesh connectivity, and associated attributes such as coupling values on both node and element levels. Together, these machine-readable formats remove the need to parse ASCII text files and allow users to work directly with the models using the tools listed above. They allow for quantitative operations, e.g., clipping by depth, computing isosurfaces, resampling to regular grids, decimation, and provide efficient binary input/output (I/O) with compression for large models. Both the regular-grid NetCDF products and the unstructured VTU meshes integrate with standard parallel analysis and visualization tools used in high-performance computing (HPC) workflows, enabling future scalable processing of large coupling model ensembles.

Beyond the spatial formats, we collect metadata on each study's modeling choices and assumptions to provide context for every hosted coupling model. Each dataset includes metadata detailing the source publication DOI, allowing users to readily identify and cite the original studies, as well as a short description, region, and model type. The latter distinguishes between interseismic coupling models that represent time-averaged strain accumulation between earthquakes, inter-SSE models estimated during periods between slow-slip events, and kinematic block-model formulations that infer coupling from relative motions between tectonic blocks. Additional optional metadata includes the quantity and type of geodetic observations, the forward model formulation, and the inversion framework, in-

cluding parameters such as the regularization type and associated weights (see Table 1 for a list of recommended metadata). These metadata are stored both within the NetCDF file and in an accompanying YAML file (Ben-Kiki et al., 2009), whose hierarchical structure separates observational, forward-model, and inversion information into human- and machine-readable records of model parameters. Lastly, when available, we include the original observed geodetic fields and associated uncertainties in ASCII format as part of the model dataset. All CC data products, including NetCDF coupling values, VTU geometries, YAML metadata, and geodetic observations are freely accessible through the CC interface as well as an example Jupyter notebook that demonstrates data access, metadata parsing, and visualization.

4 The Coupling Cloud platform

4.1 Platform architecture

The CC platform operates on a virtual machine within an eight-node Proxmox virtualization cluster hosted at the Scripps Institution of Oceanography, University of California San Diego. The system is configured with two virtual CPUs and 8 GB of RAM, running AlmaLinux 9.6, with Apache serving the web application and a FastAPI backend that handles all dynamic data requests (Fig. 1). The CC features two viewers: a 2D map viewer and a 3D geometry viewer. The 2D viewer displays surface-projected coupling values in a map interface and uses real-time server-side tiling via TiTiler, which converts NetCDF datasets into “tiles”, small image segments, at multiple zoom levels that form the full map. These tiles are added as data layers in Leaflet, an open-source JavaScript library that renders the interactive basemap and enables users to explore and compare coupling fields in geographic context.

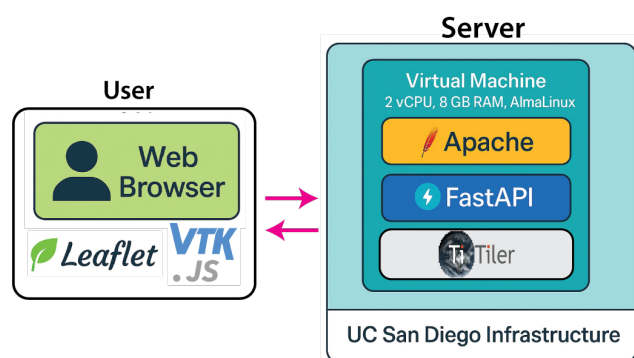


Figure 1 CC platform architecture describing the server and user sides.

The 3D viewer provides an interactive environment for exploring coupling fields on the original plate-interface geometry. For models where the slab depth is available, we construct 3D representations of the interface by converting geographic coordinates (latitude, longitude, and depth) to Earth-Centered Earth-Fixed coordinates and exporting the resulting surfaces as VTK PolyData (.vtp) files (Schroeder et al., 1998). The Cou-

pling Cloud 3D viewer loads these files directly in a browser using `vtk.js` (Fig. 1), an open-source JavaScript library for scientific visualization. For each subduction zone, the 3D viewer includes an Earth surface layer derived from GEMCO (Becker et al., 2009), providing geographic context as users rotate, zoom, and explore coupling models, the megathrust interface and the overlying topography.

4.2 User interface and workflow

The CC is a browser-based workspace for finding, visualizing in 2D and 3D, comparing, and downloading published kinematic coupling models across subduction zones. Using the 2D viewer, users can select a margin from the dataset panel, display one or several models for that region, and compare their spatial distributions by toggling through layers, and adjusting the colorbar, allowing for examination of differences in the extent of coupling (Fig. 2A). In addition to the coupling fields, the CC documents supplementary fields such as uncertainty, which can become substantial where geodetic constraints are sparse, particularly in offshore regions (e.g., DeSanto et al., 2025; Lindsey et al., 2021; Nishimura et al., 2018). If provided, users can visualize these uncertainty data sets alongside the coupling maps (Fig. 2B) or download them, allowing assessment of the reliability of specific features and propagation of uncertainty into their own analyses.

Kinematic coupling models assume plate-interface geometries that range from planar surfaces to detailed 3D geometries, often based on the Slab2 model (Hayes et al., 2018), which may lead to variations in the inferred slip deficit distributions (Baba et al., 2002; Elston et al., 2025; Moreno et al., 2009). Within the CC 2D viewer, users can visualize and compare these geometric choices (Fig. 3C). In addition to the 2D viewer, the CC includes a 3D viewer for visualizing coupling on the 3D plate-interface geometry. Users can activate the 3D view by selecting a subduction zone and entering its 3D view, where all models with available geometry can be explored (Fig. 3). This tool provides an intuitive way to examine how geometric assumptions influence inferred coupling, complementing the 2D surface view and enhancing comparison across models that use different representations of the plate interface. Users can download dislocation geometries as VTU files for offline visualization and analyses.

Variability among kinematic coupling models arises from differences in inversion setup and observational constraints (Avouac, 2015; Kaneko et al., 2010). These differences include the geodetic measurement tools used, ranging from GNSS to InSAR, leveling, paleogeodetic, and offshore measurements, as well as the time periods over which interseismic velocities are estimated and how aseismic processes such as postseismic deformation and interseismic transients are treated (Bürgmann et al., 2000; Chlieh et al., 2008; Dixon, 1991; Gagnon et al., 2005; Jackson and Bilham, 1994). The inversion strategies themselves span regularized least-squares formulations to fully Bayesian frameworks that explicitly probe the posterior distribution. Differences

Parameter	Description
Model type	Interseismic/Inter-SSE/Block model or a combination of these.
Inversion type	Method of inversion used (e.g. Tikhonov regularization, Bayesian, stochastic Bayesian, least-squares).
Forward model formulation	Earth model used to compute surface displacement, such as a uniform elastic half-space, layered elastic structure, or a viscoelastic rheology.
Type of dislocation	Geometry of the dislocation elements (triangular, rectangular, or piecewise-linear triangular).
Number of dislocations	Total number of dislocation elements used in the forward model.
Degrees of freedom	Total number of parameters solved for in the inversion.
Type of Observations	Type(s) of geodetic observations used (e.g., Campaign GNSS, permanent GNSS, InSAR, leveling, coral etc.).
Observation Components	East/North/Up (or E/N/U)
Number of sites	Number of sites (or pixels in case of InSAR) used in the inversion.
Number of observations	Total number of individual observation components (e.g., if one site uses North/East components and another uses Up/Down, the total is 3).
Reference frame	Global geodetic reference frame (e.g., ITRF2014, ITRF2008).
Plate-fixed frame	Tectonic or plate-relative reference frame used to interpret interseismic deformation (e.g., Australian plate) including when possible.
Earliest data used	Start date of the geodetic observations incorporated in the inversion (format: YYYY or YYYY-MM or YYYY-MM-DD).
Latest data used	End date of the geodetic observations incorporated in the inversion (format: YYYY or YYYY-MM or YYYY-MM-DD).
Regularization type	Form of regularization applied during the inversion (e.g., Laplacian smoothing, Tikhonov regularization. etc.).
Smoothing weight	Value of the regularization weights used in the inversion.
Smoothing length scales	Value of length scale used in the regularization.
Couple values computed	Indicates whether coupling was computed at dislocation nodes or over full dislocation patches.
Poisson ratio	Value of the Poisson's ratio assumed if a single layer model is used.
Number of layers	Number of layers used in the model, if applicable.
Convergence model	Relative plate velocity model (required for normalization of slip deficit to obtain coupling)
Kinematic constraints	A priori assumptions about slip deficit rate (e.g., rake direction).

Table 1 Recommended metadata fields for coupling models.

in regularization schemes and associated weights, fault parameterization, a priori constraints (e.g., imposed creep at depth or fixed rake), the adopted kinematic block models and plate reference frame further influence the inferred coupling distribution (Loverly et al., 2024; Métois et al., 2016; Villegas-Lanza et al., 2016).

These methodological differences also reflect that the quantity referred to as “kinematic coupling” is not defined identically across all studies. For example, in regions experiencing slow-slip events, some studies estimate long-term interseismic coupling, whereas others estimate coupling only during intervals between slow-slip episodes (e.g. Maubant et al., 2023; Michel et al., 2025; Radiguet et al., 2016). In classical backslip formulations (Savage, 1983), coupling is inferred by relating surface deformation to slip deficit through elastic half-space dislocation models. In contrast, viscoelastic earthquake-cycle models infer coupling using forward models that account for time-dependent viscous deformation, which can yield different coupling distributions even for the same geodetic observations. Block-

model approaches derive coupling by simultaneously estimating relative block motions and slip deficit on the megathrust interface. To document such differences, we compiled metadata for each model that can be viewed directly on the platform (Fig. 4) or downloaded as YAML files. Users should consult these metadata, particularly the model type, forward-model formulation, inversion framework and other metadata (Table 1), as well as the original publications, before interpreting or comparing models.

4.3 Performance

We evaluate the responsiveness and scalability of the Coupling Cloud platform during interactive use, where the computational demand is highest. Initial page loads are fast, on the order of ~1 second for up to about ten simultaneous users, because only a small amount of data is transferred during the initial page load. The primary computational load arises from 2D tile requests during user interaction, so we benchmark the number of

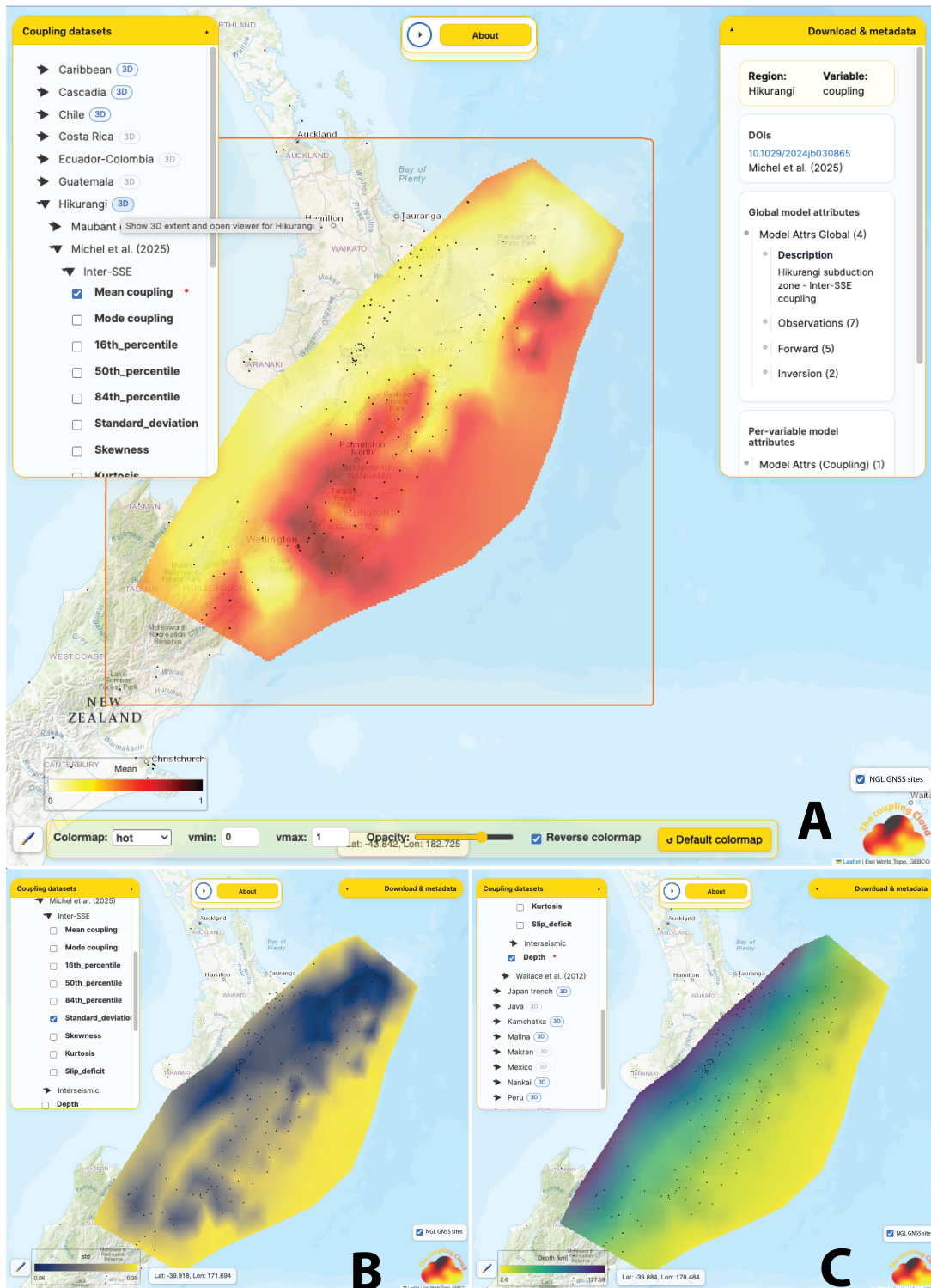


Figure 2 Coupling Cloud 2D viewer overview. The 2D viewer provides an interactive map-based interface for exploring kinematic coupling models and their associated metadata. Users can select models, adjust visualization settings, and switch seamlessly between the 2D and 3D viewers. A. The upper-left panel shows the dataset selector, which allows users to choose coupling models to display in the 2D map viewer. The 3D button switches to the 3D viewer, with the red polygon indicating the region covered by the 3D viewer. The lower-left panel contains the brush controls used to configure colormap settings. The upper-right panel displays the metadata associated with the selected coupling model, and a link to download the dataset. The “About” panel contains the full reference list and additional platform information. Black dots indicate the position of GNSS stations associated with time series in the Nevada Geodetic Laboratory (NGL). Examples showing the selection of supplementary fields, including standard deviation and interface depth, for the same coupling model in Hikurangi (Michel et al., 2025).

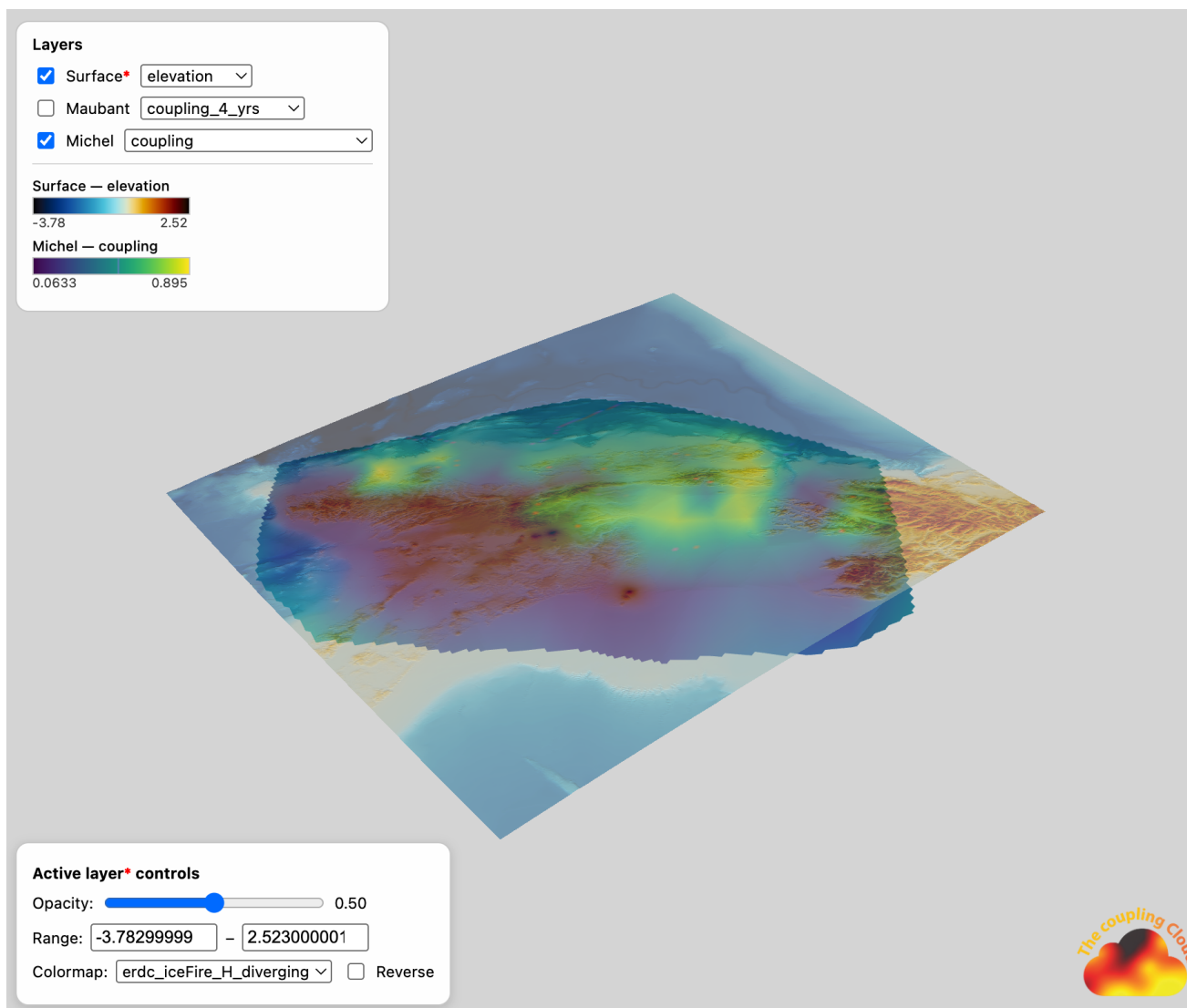


Figure 3 Coupling Cloud 3D viewer overview. The 3D viewer enables interactive exploration of coupling models on the actual plate-interface geometry used in each inversion. It displays the megathrust surface in Earth-centered coordinates and overlays Earth-surface layer that provides geographic context. Users can select which geometric or coupling layers to display and customize their colormaps and opacity settings through the *Layers* and *Active Layers* control panels. The example shown here is from the Hikurangi subduction zone, illustrating the coupling field for the same model displayed in Fig. 2 with the horizontal extent of the surface layer matching the red polygon shown in Fig. 2A.

concurrent requests the backend can sustain. We issue 3,000 requests for the same tile at progressively increasing concurrency levels and measure the time required for TiTiler to serve all requests. Under our current configuration, which includes two virtual CPUs and 8 GB of RAM, the total processing time decreases with increasing concurrency as CPU resources are utilized more fully, until it reaches a plateau where the server is operating at maximum capacity with sustaining a throughput of approximately 45 tile requests per second (Fig. 5). A typical 2D map viewer user interaction such as panning or zooming triggers approximately 15 new tile requests. In practice, tile caching means that retrieved tiles are stored locally in the user's browser. Thus, interactions within already viewed areas impose no additional load on the backend, and the CC 2D viewer can support many more users than implied by the baseline throughput for uncached tiles.

Even in cases where the dynamic server becomes

slow to respond due to high user load, our benchmark demonstrates that the architecture is scalable at least for small numbers of CPUs. A single-CPU configuration delivers roughly half the throughput of the two-CPU setup (Fig. 5), indicating near-linear performance scaling in this test. This suggests that adding additional CPU resources can increase system capacity, with the caveat that allocating more virtual CPUs incur higher purchasing and maintenance costs. We highlight that the 3D viewer requires no backend computation, as all visualization is handled directly in the user's browser. The only server-side operation is transferring the VTK PolyData geometry files to the client, which are typically a few megabytes in size and load within seconds, depending on the user's internet connection.

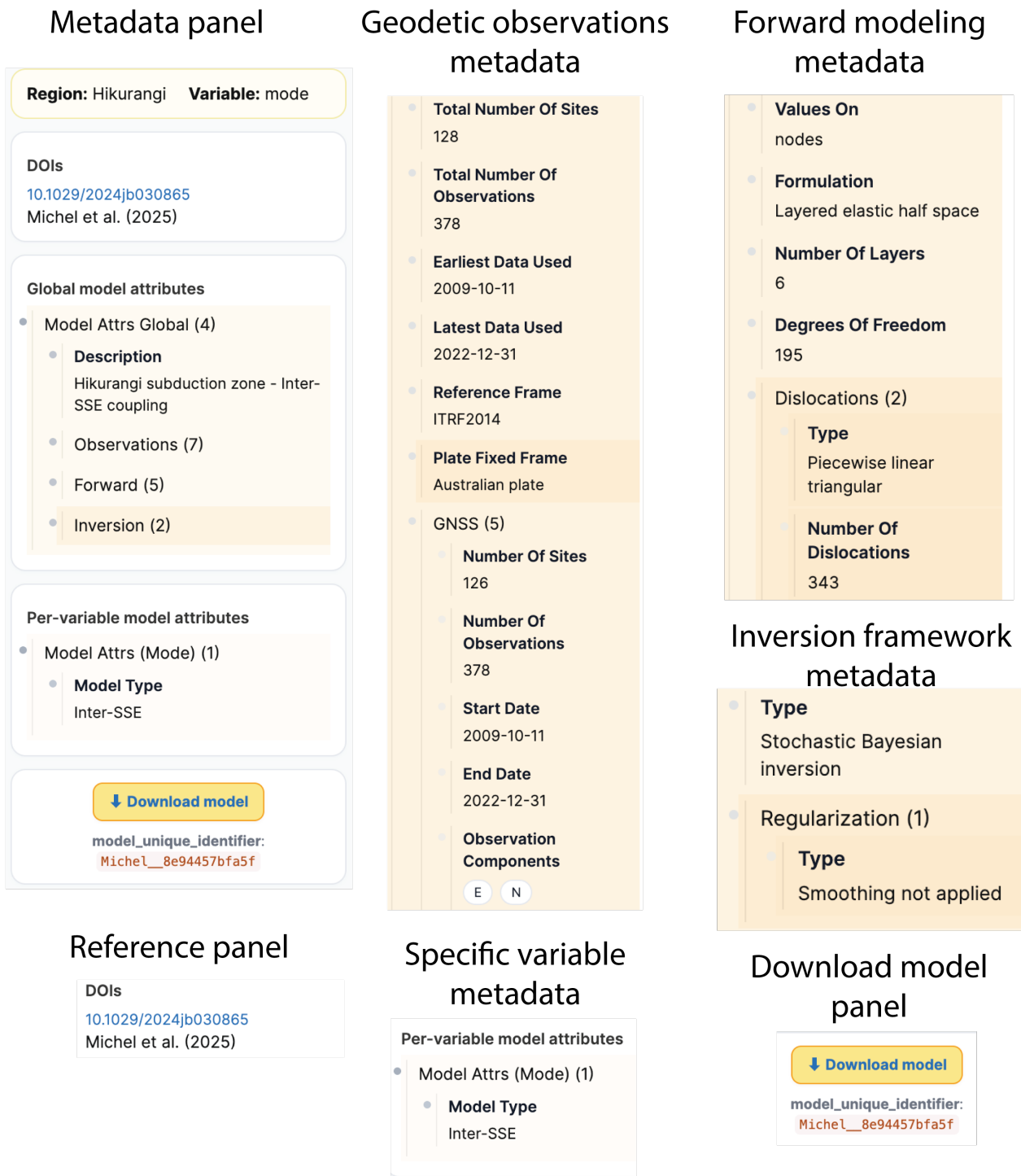


Figure 4 Example of the metadata interface in the Coupling Cloud platform. The metadata panel provides a detailed hierarchical summary of each coupling model, including DOIs, global attributes, per-variable attributes, observational constraints, forward-model settings, and inversion parameters. Shown here is the complete metadata for the Hikurangi coupling model of Michel et al. (2025), organized into its main components: the reference, observations, forward model, inversion, per-variable metadata, and download.

5 A simple demonstration: along-strike segmentation of the Cascadia megathrust in kinematic coupling models

To illustrate the advantages of assembling many published coupling models within a single standardized framework, we present a case study for the Cascadia subduction zone. The CC currently aggregates eight

full-margin Cascadia interseismic coupling models that include plate-interface depth information (Fig. 6A). These models span more than a decade of geodetic inversion studies and employ a range of elastic, viscoelastic, and boundary-based forward and inverse modeling approaches, including regularized, parameterized slip-rate deficit inversions (Schmalzle et al., 2014), regularized linear inversions (Michel et al., 2018), regularized inversions with physical constraints (Lindsey et al.,

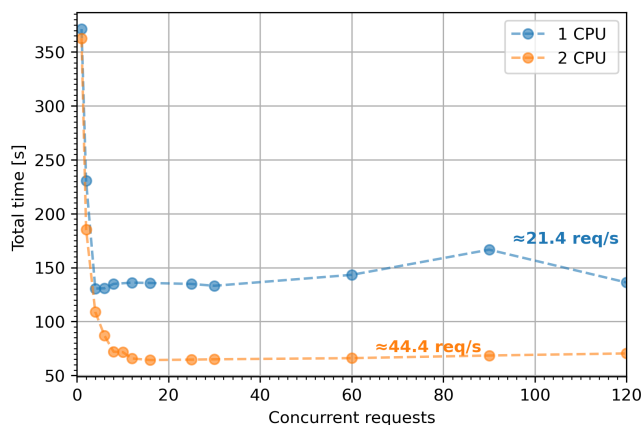


Figure 5 Coupling Cloud backend performance benchmark showing response times for increasing levels of concurrent tile requests. Points show the total time required to process 3,000 HTTP tile requests under different CPU configurations and concurrency levels.

2021), Bayesian boundary inversions (Sherrill et al., 2024), and viscoelastic earthquake-cycle modeling (Pollitz and Evans, 2017; Pollitz, 2025). As a brief example of the utility of the CC platform, we view these models together (Fig. 6A1–8) to assess how their inferred coupling distributions relate to proposed along-strike segmentation of the Cascadia margin.

Whether a megathrust is segmented along strike controls rupture behavior and whether slip deficit is released in single margin-wide earthquakes or in a sequence of smaller events (e.g., Arnulf et al., 2022; Bassett et al., 2025; Melnick et al., 2009; Philiposian and Meltzner, 2020). Cascadia is a classic example where this question remains central (e.g., Melgar, 2021). Slow-slip and tremor catalogs reveal along-strike sections whose recurrence patterns and spatial distributions change abruptly along strike, implying structural or frictional contrasts (Bartlow, 2020; Brudzinski and Allen, 2007). High-resolution seismic imaging reveals sharp changes in megathrust morphology that align with these inferred segment boundaries (Carbotte et al., 2024). Together with along-strike patterns in turbidite records, these observations have been interpreted as evidence for Cascadia’s along-strike segmentation, a pattern also suggested by early geodetic coupling estimates, with higher coupling in the northern and southern segments and lower coupling in the central portion (Goldfinger et al., 2012; Schmalzle et al., 2014).

We define three commonly used along-strike subsections of the Cascadia margin (e.g., Ramos et al., 2021): a northern segment (Vancouver Island to $\sim 46^\circ$ N), a central segment ($\sim 46\text{--}43.5^\circ$ N), and a southern segment ($\sim 43.5^\circ$ N to Mendocino Triple Junction). For each model, we extract Coupling Cloud–stored gridded coupling values shallower than 20 km, where along-strike variations in coupling are most commonly inferred (Fig. 6A1–2). These values correspond to spatially distinct fault patches within each along-strike segment. We describe how coupling values are distributed across these spatial units by computing a probability density function (PDF) for each model and segment (e.g., Oryan

and Gabriel, 2025) using a Gaussian kernel density estimator with bandwidth selected according to Scott’s rule (Scott, 1979). We note that the PDF is used as a normalized representation of the density and relative weighting of coupling values across the coupling spectrum and not as a result of repeated measurements of a stochastic process. Finally, we express each segment’s PDF as a deviation from the margin-wide PDF for the same model, so that positive deviations highlight coupling values that are overrepresented within a given segment relative to the margin as a whole.

Our analysis shows little sensitivity to kernel bandwidth and grid resolution, and reveals that the northern-segment PDF curve rises by up to ~ 1 in probability density above the margin-wide PDF at coupling values larger than 0.7. This indicates that high-coupling values are more concentrated in the northern segment than across the Cascadia subduction zone as a whole. Similarly, the central segment PDF remains below the margin-wide PDF for coupling values larger than ~ 0.8 , indicating a lower density of high-coupling values relative to the margin-wide distribution (Fig. 6B2). In contrast, the southern segment does not show a higher concentration of high coupling values, and its PDF remains below the margin-wide distribution, reaching negative deviations of up to ~ 1 in probability density, similar in magnitude to the positive deviations observed in the northern segment (Fig. 6B3).

This example averages distributions across multiple coupling models spanning a range of inversion strategies and forward-modeling approaches. These models are not strictly independent, however, as they share geodetic datasets and related regularization strategies, and the ensemble spread should not be interpreted as a quantitative measure of uncertainty. Rather, the ensemble is intended to illustrate first-order behavior rather than provide a formal statistical treatment of inter-model variability and uncertainty. Even so, it shows that the concentration of coupling values in the northern and central segments aligns with previous interpretations of Cascadia’s along-strike segmentation (Brudzinski and Allen, 2007; Carbotte et al., 2024; Goldfinger et al., 2012), whereas the southern segment does not exhibit a similarly coherent high-coupling pattern. This example also demonstrates how synthesizing ensemble models within the Coupling Cloud framework could help distinguish features that persist across modeling approaches from those that may depend on individual methodological choices. We therefore urge users to use the associated metadata and uncertainty information when comparing models and, most importantly, to consult the original publications describing each model, where the underlying assumptions and methodological choices are fully documented.

6 Current and future roles of the Coupling Cloud platform

The CC is designed with long-term sustainability in mind, hosted at Scripps / UC San Diego’s institutional infrastructure with redundant backups and grounded

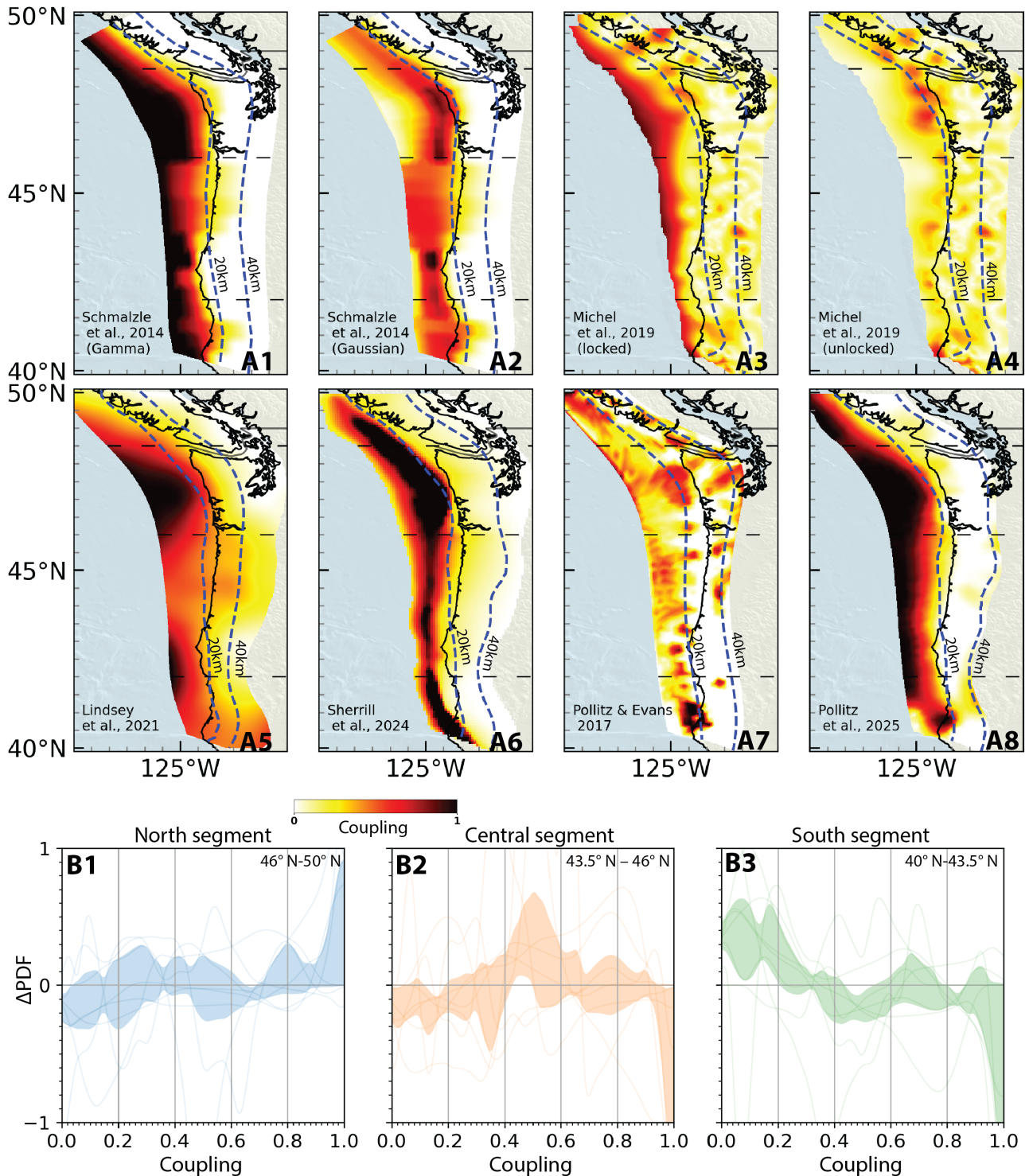


Figure 6 Cascadia case study. A - Eight Cascadia wide interseismic coupling models with slab depth available on the CC platform (Lindsey et al., 2021; Pollitz and Evans, 2017; Pollitz, 2025; Schmalzle et al., 2014; Sherrill et al., 2024; Michel et al., 2018), shown for interface depths shallower than 60 km. Contours indicate the megathrust interface depth used in each model. Horizontal dashed lines mark segments. B - Thin curves show the deviation of each model’s segment-specific coupling probability density from that model’s margin-wide probability density (Δ PDF). Positive Δ PDF values indicate coupling values that are more frequent within a given segment than across the margin. The shaded band denotes the 25th–75th percentile range of Δ PDF across the eight models.

in stable, widely supported data formats and libraries, ensuring continued accessibility and minimal maintenance. Our goal is for the CC to serve as a long-term community-driven global repository for kinematic cou-

pling models, an up-to-date archive that the community can rely on for synthesis, comparison, and reproducibility. We also envision the CC to form a valuable teaching resource, offering standardized datasets for

training the next generation of geodesists and subduction zone scientists, as well as providing an easy entry point for researchers new to the field. In addition, the platform is extensible and supports user-driven uploads, allowing researchers to easily contribute new coupling models, metadata, and geometries directly. We invite all authors preparing new or forthcoming coupling models to upload their datasets to the CC so that the community can benefit from timely, open, and standardized access to the latest coupling models.

In addition, we hope that the unified file formats adopted here, NetCDF for surface-projected coupling fields, VTU (VTK PolyData) for plate-interface dislocation geometries, and YAML for FAIR-compliant metadata, will help providing a working standard for the community. By encouraging authors to express new coupling models directly in these formats, we aim to streamline data exchange and improve reproducibility across tools and research groups. At the same time, if the community converges on alternative standards, the CC framework can readily adopt them through simple import workflows, ensuring continued support for whichever formats best serve the megathrust research community.

Looking ahead, we see the Coupling Cloud not only as a repository of coupling models but as an evolving platform designed to reduce methodological variability and to bridge our understanding of how slip is accumulated and released in subduction zones (e.g., Wang et al., 2012). One promising direction is to host community validated Green's functions for subduction margins (e.g., Hori et al., 2021), providing a consistent set of forward-modeling kernels that removes a major source of variability among existing coupling models (Li et al., 2015; Lavery et al., 2025; Wang et al., 2021). A near-term direction for future developments is to link coupling models more directly to the geodetic observations used in the underlying inversions. Although users can already download the coupling-model associated observational datasets, if available, future versions of the CC may place greater emphasis on graphical representation, e.g., allowing GNSS velocities and time series, InSAR displacement fields, and offshore GNSS-Acoustic measurements to be viewed alongside coupling fields.

Finally, seamless integration of the CC interseismic coupling archive with the SRCMOD coseismic slip repository (Mai and Thingbaijam, 2014) and the Slow Earthquake Database (Kano et al., 2018) would unify complementary perspectives on megathrust behavior. Realizing this vision would require transforming the text-based FSP (Mai et al., 2016b) and CSV formats used by SRCMOD and Slow Earthquake Databases into the VTU and NetCDF formats adopted by the Coupling Cloud, harmonizing metadata structures across both archives, and establishing an interface that links ruptures and slow slip events to corresponding interseismic coupling models. With such integration, users could examine coseismic and slow earthquake slip distributions alongside interseismic coupling fields, offering a unified perspective on strain accumulation and release across the earthquake cycle.

7 Conclusions

We have developed the Coupling Cloud, a unified and FAIR-compliant platform for standardizing, distributing, visualizing, and comparing kinematic geodetic coupling models across global subduction zones. The CC currently hosts 96 coupling models from 55 publications covering 21 subduction margins, each standardized into common file formats with preserved plate-interface geometries and complete metadata. By providing interactive 2D and 3D visualization tools and unified formats, the platform aims to remove long-standing barriers to reproducibility and to enable more transparent comparison among models constructed with differing data sets and methodologies, while associated metadata enables users to consult the original publications for methodological details. As the Coupling Cloud grows through community contributions and future integration of observational datasets and models, it is well positioned to serve as a long-lived resource for advancing understanding of megathrust deformation and seismic hazard.

Acknowledgements

We thank the Editor Dr. Wenbin Xu and two anonymous reviewers for their constructive feedback. We also thank Kathryn Materna, Fred Pollitz, Eileen Evans, Jean-Philippe Avouac and Adriano Gualandi for sharing their coupling models. The Coupling Cloud server was built using TiTiler (<https://github.com/developmentseed/titiler>), FastAPI (<https://github.com/fastapi/fastapi>), Leaflet (<https://leafletjs.com/>) and vtk.js (<https://kitware.github.io/vtk-js/docs/>). B.O. and A.G. acknowledges support from the IGPP Green Foundation, National Science Foundation (grant no. OAC-2311208) and CRESCENT Award 2017Y0SD. A.G. further acknowledges support from Horizon Europe (ChEESE-2P, grant number 101093038 and Geo-INQUIRE, grant number 101058518), NSF (grant nos. OAC-2139536, EAR-2225286, EAR-2121568, RISE-2531036) and the Statewide California Earthquake Center (SCEC grants #25313, 25259). E.C. thanks the IGS, UNAVCO, Institut Universitaire de France and the FEDER European Community program within the Interreg Caraïbes "PREST" project. M.C. and C.D. acknowledge the Agence Nationale de la Recherche (ANR-07-BLAN-0143-01) and the IRD. B.C. and C.D. acknowledge NSF grants EAR-9526419, EAR-9804905, EAR-9909321, EAR-0510553, EAR-1114174, the University of Wisconsin-Madison and the UW-Madison Department of Geoscience Weeks endowment funds. L.D. and L.F. acknowledge Singapore Ministry of Education Tier 3b project "Investigating Volcano and Earthquake Science and Technology (InVEST)" (MOE-MOET32021-0002). A.E. acknowledges UNAVCO Graduate COCONet Fellowship and NSF grant EAR-1144418. J.T.F. acknowledges NSF grant EAR-1457361, and USGS grant G15AP00051. E.G. acknowledges the Ministry of Higher Education, Science and Technology of Indonesia (Kemendikisaintek). N.R.H. acknowledges Geospatial Information Agency of Indonesia, MEXT scholarship, Nagoya University, and Research and Innovation for Advanced Indonesia (RIIM) scheme. Y.H. acknowl-

edges grant AS-102-SS-A09 and MOST 102-2116-M-001-028-MY3. T.I. acknowledges support from the Japan Society of the Promotion of Science (JSPS) Grants-in Aid for Scientific Research (KAKENHI) grants JP21H05200 and JP16H06472. J.J. acknowledges Chilean National Science Cooperation (CONICYT) through “Becas Chile” Program and MSCA Postdoctoral Fellowship (MSCA-101066069, project ERASMUS). R.J. acknowledges support from the Institut Universitaire de France and the European Research Council (ERC) under the European Union’s Horizon 2020 research and innovation program (Grant Agreement 758210 and 805256, Geo4D and iQuake projects) as well as NASA (Grant NNX16AK58G). E.K. acknowledges the French-Chilean LiA ‘Montessus de Ballore’, the Agence Nationale de la Recherche (ANR-2012-BS06-004) and the French INSU Tellus program, all data were collected by the instruments of the French mobile GNSS park GPSMob of Epos-France managed by CNRS Terre & Univers. S.M. acknowledges the ERC under the European Union’s Horizon 2020 research and innovation program (Grant 758210 for project Geo4D). S.M. acknowledges NSF award EAR-1821853. M.M. acknowledges the French-Chilean LiA “Montessus de Ballore”, CNRS, MAE, IPGP, UJF and ANR project MEGA-Chile (project number 12-BS06-004). R.P. acknowledges DGAPA–UNAM PAPIIT project IA104525. E.M.S. thanks NSF grants EAR-2121631 and EAR-2045291 and USGS grant G20AP00017, and in part by Lilly Endowment, Inc., through its support for the Indiana University Pervasive Technology Institute. J.V.-L. acknowledges the Agence Nationale de la Recherche (ANR-07-BLAN-0143-01) and IRD and the Instituto Geofísico del Perú (IGP). E.O.L. acknowledges support from NSF grant OCE-2314273 and NASA (grant 80NSSC23K0654). B.L. acknowledges support from the French national space agency (CNES). A.S. acknowledges support from the ERC Consolidator grant 865963 DEEP-trigger. Instrumentation and data from OVSICORI-UNA used in this research was supported by Costa Rican Emergency Law 8933 and by Universidad Nacional de Costa Rica through the project 0097–2020 “Sistema de monitoreo geodésico (SiMoGeod) de los volcanes y de la tectónica de Costa Rica.” D.P. thanks the United States-India Educational Foundation (USIEF) for the financial support through the Fulbright-Nehru Postdoctoral Research Programme (Award 2783 FNPDR/2022). L.M. acknowledges support from NASA under Grant No.~80NSSC21K0874. S.Y. acknowledges support by JSPS KAKENHI grants JP15H01140, JP16H06477 and JP21H05203, and The Project for Hazard Assessment of Large Earthquakes and Tsunamis in the Mexican Pacific Coast for Disaster Mitigation, SATREPS funded by JST-JICA (#1554361). M.R. acknowledges support by the Agence Nationale de la Recherche (ANR21-CE49-0023) SSDYN project. Y.I. acknowledges JSPS KAKENHI grant JP17J00173 and Kyoto University Foundation. T.N. acknowledges JSPS KAKENHI grants JP21H05200, JP16H06472, JP15K21755 and JP26109007. Z. L. acknowledges support from NASA’s Earth Surface and Interior Focus Area. Part of the work was carried out at the Jet Propulsion Laboratory, California Institute of Technology, under a contract with the National Aeronautics and Space Administration

(80NM0018F0591). We acknowledge GNSS data from Alaska and Cascadia provided by the NSF-supported GAGE Facility (awards 1724794, 1724509).

7.1 Data and code availability

All coupling datasets are freely available to download from couplingcloud.ucsd.edu. The code to run the coupling cloud can be found in [Oryan \(2025\)](https://zenodo.org/records/17821569) (<https://zenodo.org/records/17821569>).

7.2 Competing interests

All authors declare no competing interests.

References

- Abe, D. and Yoshioka, S. Spatiotemporal distributions of interplate coupling in Tohoku, northeast Japan, for 14 years prior to the 2011 Tohoku-oki earthquake inverted from GNSS data. *Tectonophysics*, 838, 2022. doi: [10.1016/j.tecto.2022.229479](https://doi.org/10.1016/j.tecto.2022.229479).
- Ahrens, J., Geveci, B., and Law, C. *ParaView: An End-User Tool for Large-Data Visualization*, page 717–731. Elsevier, 2005. doi: [10.1016/b978-012387582-2/50038-1](https://doi.org/10.1016/b978-012387582-2/50038-1).
- Arnulf, A. F., Bassett, D., Harding, A. J., Kodaira, S., Nakanishi, A., and Moore, G. Upper-plate controls on subduction zone geometry, hydration and earthquake behaviour. *Nature Geoscience*, 15(2):143–148, Feb. 2022. doi: [10.1038/s41561-021-00879-x](https://doi.org/10.1038/s41561-021-00879-x).
- Avouac, J.-P. From Geodetic Imaging of Seismic and Aseismic Fault Slip to Dynamic Modeling of the Seismic Cycle. *Annual Review of Earth and Planetary Sciences*, 43(1):233–271, May 2015. doi: [10.1146/annurev-earth-060614-105302](https://doi.org/10.1146/annurev-earth-060614-105302).
- Baba, T., Tanioka, Y., Cummins, P. R., and Uhira, K. The slip distribution of the 1946 Nankai earthquake estimated from tsunami inversion using a new plate model. *Physics of the Earth and Planetary Interiors*, 132(1-3), 2002. doi: [10.1016/s0031-9201\(02\)00044-4](https://doi.org/10.1016/s0031-9201(02)00044-4).
- Bartlow, N. M. A Long-Term View of Episodic Tremor and Slip in Cascadia. *Geophysical Research Letters*, 47(3), Feb. 2020. doi: [10.1029/2019gl085303](https://doi.org/10.1029/2019gl085303).
- Bassett, D., Shillington, D. J., Wallace, L. M., and Elliott, J. L. Variation in slip behaviour along megathrusts controlled by multiple physical properties. *Nature Geoscience*, 18(1):20–31, Jan. 2025. doi: [10.1038/s41561-024-01617-9](https://doi.org/10.1038/s41561-024-01617-9).
- Becker, J. J., Sandwell, D. T., Smith, W. H. F., Braud, J., Binder, B., Depner, J., Fabre, D., Factor, J., Ingalls, S., Kim, S.-H., Ladner, R., Marks, K., Nelson, S., Pharaoh, A., Trimmer, R., Von Rosenberg, J., Wallace, G., and Weatherall, P. Global Bathymetry and Elevation Data at 30 Arc Seconds Resolution: SRTM30_PLUS. *Marine Geodesy*, 32(4):355–371, Nov. 2009. doi: [10.1080/01490410903297766](https://doi.org/10.1080/01490410903297766).
- Ben-Kiki, O., Evans, C., and Ingerson, B. *YAML Ain’t Markup Language (YAML) Version 1.1*, 2009. <https://yaml.org/spec/1.1/>. Working Draft.
- Blewitt, G., Hammond, W., and Kreemer, C. Harnessing the GPS Data Explosion for Interdisciplinary Science. *Eos*, 99, 2018. doi: [10.1029/2018eo104623](https://doi.org/10.1029/2018eo104623).
- Brudzinski, M. R. and Allen, R. M. Segmentation in episodic tremor and slip all along Cascadia. *Geology*, 35(10):907, 2007. doi: [10.1130/g23740a.1](https://doi.org/10.1130/g23740a.1).
- Burgette, R. J., Weldon, R. J., and Schmidt, D. A. Interseismic uplift rates for western Oregon and along-strike variation in locking on the Cascadia subduction zone. *Journal of Geophysical Research: Solid Earth*, 114(B1), Jan. 2009. doi: [10.1029/2008jb005679](https://doi.org/10.1029/2008jb005679).

- Bürgmann, R., Rosen, P. A., and Fielding, E. J. Synthetic Aperture Radar Interferometry to Measure Earth's Surface Topography and Its Deformation. *Annual Review of Earth and Planetary Sciences*, 28(1):169–209, May 2000. doi: 10.1146/annurev.earth.28.1.169.
- Bürgmann, R., Kogan, M. G., Steblov, G. M., Hilley, G., Levin, V. E., and Apel, E. Interseismic coupling and asperity distribution along the Kamchatka subduction zone. *Journal of Geophysical Research: Solid Earth*, 110(B7), 2005. doi: 10.1029/2005jb003648.
- Carbotte, S. M., Boston, B., Han, S., Shuck, B., Beeson, J., Canales, J. P., Tobin, H., Miller, N., Nedimovic, M., Tréhu, A., Lee, M., Lucas, M. C., Jian, H., Jiang, D., Moser, L., Anderson, C., Judd, D., Fernandez, J., Campbell, C., Goswami, A., and Gahlawat, R. Subducting plate structure and megathrust morphology from deep seismic imaging linked to earthquake rupture segmentation at Cascadia. *Science Advances*, 10(23), 2024. doi: 10.1126/sciadv.adl3198.
- Cheng, G., Barnhart, W. D., and Small, D. Constraints from GPS measurements on plate coupling within the Makran subduction zone and tsunami scenarios in the western Indian Ocean. *Geophysical Journal International*, 237(1):288–301, Feb. 2024. doi: 10.1093/gji/ggae046.
- Chlieh, M., Avouac, J. P., Sieh, K., Natawidjaja, D. H., and Galetzka, J. Heterogeneous coupling of the Sumatran megathrust constrained by geodetic and paleogeodetic measurements. *Journal of Geophysical Research: Solid Earth*, 113(B5), May 2008. doi: 10.1029/2007jb004981.
- Chlieh, M., Beauval, C., Yepes, H., Marinière, J., Saillard, M., and Audin, L. Seismic and Aseismic Cycle of the Ecuador–Colombia Subduction Zone. *Frontiers in Earth Science*, 9, 2021. doi: 10.3389/feart.2021.701720.
- Cosenza-Murales, B., DeMets, C., Márquez-Azúa, B., Sánchez, O., Stock, J., Cabral-Cano, E., and McCaffrey, R. GPS-derived interseismic fault locking along the Jalisco–Colima segment of the Mexico subduction zone. *Geophysical Journal International*, 228(3):2174–2197, Oct. 2021. doi: 10.1093/gji/ggab436.
- Cruz-Atienza, V. M., Tago, J., Domínguez, L. A., Kostoglodov, V., Ito, Y., Ovando-Shelley, E., Rodríguez-Nikl, T., González, R., Franco, S., Solano-Rojas, D., Beltrán-Gracia, J., Miranda-García, P., Boudin, F., Rivera, L., Bécel, A., Villafuerte, C., Real, J., Kazachkina, E., and Ronquillo, A. Seafloor geodesy unveils seismogenesis of large subduction earthquakes in Mexico. *Science Advances*, 11(37), 2025. doi: 10.1126/sciadv.adu8259.
- Dal Zilio, L., Jolivet, R., and van Dinther, Y. Segmentation of the Main Himalayan Thrust Illuminated by Bayesian Inference of Interseismic Coupling. *Geophysical Research Letters*, 47(4), Feb. 2020. doi: 10.1029/2019gl086424.
- DeSanto, J. B., Schmidt, D. A., Zumberge, M., Sasagawa, G., and Chadwell, C. D. Near full locking on the shallow megathrust of the central Cascadia subduction zone revealed by GNSS-Acoustic. *Earth and Planetary Science Letters*, 665, 2025. doi: 10.1016/j.epsl.2025.119463.
- Dixon, T. H. An introduction to the global positioning system and some geological applications. *Reviews of Geophysics*, 29(2): 249–276, May 1991. doi: 10.1029/91rg00152.
- Drooff, C. and Freymueller, J. T. New Constraints on Slip Deficit on the Aleutian Megathrust and Inflation at Mt. Veniaminof, Alaska From Repeat GPS Measurements. *Geophysical Research Letters*, 48(4), Feb. 2021. doi: 10.1029/2020gl091787.
- Ellis, A., DeMets, C., McCaffrey, R., Briole, P., Cosenza Murales, B., Flores, O., Guzmán-Speziale, M., Hernández, D., Kostoglodov, V., LaFemina, P., Lord, N., Lasserre, C., Lyon-Caen, H., Rodríguez Maradiaga, M., Molina, E., Rivera, J., Rogers, R., Staller, A., and Tikoff, B. GPS constraints on deformation in northern Central America from 1999 to 2017, Part 2: Block rotations and fault slip rates, fault locking and distributed deformation. *Geophysical Journal International*, 218(2):729–754, Apr. 2019. doi: 10.1093/gji/ggz173.
- Elston, H. M., Loveless, J. P., and Delph, J. R. Influence of Subduction Interface Geometry on Surface Displacements and Slip Processes in Cascadia. *Earth and Space Science*, 12(10), Oct. 2025. doi: 10.1029/2025ea004623.
- Feigl, K. L., Agnew, D. C., Bock, Y., Dong, D., Donnellan, A., Hager, B. H., Herring, T. A., Jackson, D. D., Jordan, T. H., King, R. W., Larsen, S., Larson, K. M., Murray, M. H., Shen, Z., and Webb, F. H. Space geodetic measurement of crustal deformation in central and southern California, 1984–1992. *Journal of Geophysical Research: Solid Earth*, 98(B12):21677–21712, Dec. 1993. doi: 10.1029/93jb02405.
- Feng, L., Newman, A. V., Protti, M., González, V., Jiang, Y., and Dixon, T. H. Active deformation near the Nicoya Peninsula, northwestern Costa Rica, between 1996 and 2010: Interseismic megathrust coupling. *Journal of Geophysical Research: Solid Earth*, 117(B6), 2012. doi: 10.1029/2012jb009230.
- Fukuda, J. and Johnson, K. M. A Fully Bayesian Inversion for Spatial Distribution of Fault Slip with Objective Smoothing. *Bulletin of the Seismological Society of America*, 98(3), 2008. doi: 10.1785/0120070194.
- Gagnon, K., Chadwell, C. D., and Norabuena, E. Measuring the onset of locking in the Peru–Chile trench with GPS and acoustic measurements. *Nature*, 434(7030):205–208, Mar. 2005. doi: 10.1038/nature03412.
- Giardini, D., Grünthal, G., Shedlock, K. M., and Zhang, P. The GSHAP Global Seismic Hazard Map. *Annals of Geophysics*, 42(6), Nov. 1999. doi: 10.4401/ag-3784.
- Glehnman, J., Gabriel, A., Ulrich, T., Ramos, M., Huang, Y., and Lindsey, E. Partial ruptures governed by the complex interplay between geodetic slip deficit, rigidity, and pore fluid pressure in 3D Cascadia dynamic rupture simulations. *Seismica*, 2(4), 2025. doi: 10.26443/seismica.v2i4.1427.
- Goldberg, D. E., Koch, P., Melgar, D., Riquelme, S., and Yeck, W. L. Beyond the Teleseism: Introducing Regional Seismic and Geodetic Data into Routine USGS Finite-Fault Modeling. *Seismological Research Letters*, 93(6):3308–3323, Aug. 2022. doi: 10.1785/0220220047.
- Goldfinger, C., Nelson, C. H., Morey, A. E., Johnson, J. E., Patton, J. R., Karabanov, E. B., Gutierrez-Pastor, J., Eriksson, A. T., Gracia, E., Dunhill, G., Enkin, R. J., Dallimore, A., and Vallier, T. *Turbidite event history—Methods and implications for Holocene paleoseismicity of the Cascadia subduction zone*. 2012. doi: 10.3133/pp1661f.
- Gombert, B., Duputel, Z., Jolivet, R., Simons, M., Jiang, J., Liang, C., Fielding, E., and Rivera, L. Strain budget of the Ecuador–Colombia subduction zone: A stochastic view. *Earth and Planetary Science Letters*, 498, 2018. doi: 10.1016/j.epsl.2018.06.046.
- Hanifa, N. R., Sagiya, T., Kimata, F., Efendi, J., Abidin, H. Z., and Meilano, I. Interplate coupling model off the southwestern coast of Java, Indonesia, based on continuous GPS data in 2008–2010. *Earth and Planetary Science Letters*, 401, 2014. doi: 10.1016/j.epsl.2014.06.010.
- Hayes, G. P. The finite, kinematic rupture properties of great-sized earthquakes since 1990. *Earth and Planetary Science Letters*, 468, 2017. doi: 10.1016/j.epsl.2017.04.003.
- Hayes, G. P., Moore, G. L., Portner, D. E., Hearne, M., Flamme, H., Furtney, M., and Smoczyk, G. M. Slab2, a comprehensive subduction zone geometry model. *Science*, 362(6410):58–61, Oct. 2018. doi: 10.1126/science.aat4723.

- Hori, T., Agata, R., Ichimura, T., Fujita, K., Yamaguchi, T., and Inuma, T. High-fidelity elastic Green's functions for subduction zone models consistent with the global standard geodetic reference system. *Earth, Planets and Space*, 73(1), Feb. 2021. doi: 10.1186/s40623-021-01370-y.
- Hosseini, K., Matthews, K. J., Sigloch, K., Shephard, G. E., Domeier, M., and Tsekhmistrenko, M. SubMachine: Web-Based Tools for Exploring Seismic Tomography and Other Models of Earth's Deep Interior. *Geochemistry, Geophysics, Geosystems*, 19(5): 1464–1483, May 2018. doi: 10.1029/2018gc007431.
- Hoyer, S. and Hamman, J. xarray: N-D labeled Arrays and Datasets in Python. *Journal of Open Research Software*, 5(1):10, Apr. 2017. doi: 10.5334/jors.148.
- Hsu, Y., Yu, S., Loveless, J. P., Bacolcol, T., Solidum, R., Luis, A., Pelicano, A., and Woessner, J. Interseismic deformation and moment deficit along the Manila subduction zone and the Philippine Fault system. *Journal of Geophysical Research: Solid Earth*, 121(10):7639–7665, Oct. 2016. doi: 10.1002/2016jb013082.
- Hunter, J. D. Matplotlib: A 2D Graphics Environment. *Computing in Science & Engineering*, 9(3):90–95, 2007. doi: 10.1109/mcse.2007.55.
- Ide, S. *Slip Inversion*, page 193–223. Elsevier, 2007. doi: 10.1016/b978-044452748-6.00068-7.
- Itoh, Y., Nishimura, T., Wang, K., and He, J. New Megathrust Locking Model for the Southern Kurile Subduction Zone Incorporating Viscoelastic Relaxation and Non-Uniform Compliance of Upper Plate. *Journal of Geophysical Research: Solid Earth*, 126(5), May 2021. doi: 10.1029/2020jb019981.
- Jackson, M. and Bilham, R. Constraints on Himalayan deformation inferred from vertical velocity fields in Nepal and Tibet. *Journal of Geophysical Research: Solid Earth*, 99(B7), 1994. doi: 10.1029/94jb00714.
- Jara, J., Jolivet, R., Socquet, A., Comte, D., and Norabuena, E. Detection of slow slip events along the southern Peru - northern Chile subduction zone. *Seismica*, 3(1), 2024. doi: 10.26443/seismica.v3i1.980.
- Jolivet, R., Simons, M., Duputel, Z., Olive, J., Bhat, H. S., and Blettery, Q. Interseismic Loading of Subduction Megathrust Drives Long-Term Uplift in Northern Chile. *Geophysical Research Letters*, 47(8), Apr. 2020. doi: 10.1029/2019gl085377.
- Kaneko, Y., Avouac, J.-P., and Lapusta, N. Towards inferring earthquake patterns from geodetic observations of interseismic coupling. *Nature Geoscience*, 3(5):363–369, Apr. 2010. doi: 10.1038/ngeo843.
- Kano, M., Aso, N., Matsuzawa, T., Ide, S., Annoura, S., Arai, R., Baba, S., Bostock, M., Chao, K., Heki, K., Itaba, S., Ito, Y., Kamaya, N., Maeda, T., Maury, J., Nakamura, M., Nishimura, T., Obana, K., Ohta, K., Poiata, N., Rousset, B., Sugioka, H., Takagi, R., Takahashi, T., Takeo, A., Tu, Y., Uchida, N., Yamashita, Y., and Obara, K. Development of a Slow Earthquake Database. *Seismological Research Letters*, 89(4), 2018. doi: 10.1785/0220180021.
- Kano, M., Ikeuchi, A., Nishimura, T., Miyazaki, S., and Matsushima, T. Potential of megathrust earthquakes along the southern Ryukyu Trench inferred from GNSS data. *Earth, Planets and Space*, 73(1), Oct. 2021. doi: 10.1186/s40623-021-01531-z.
- Klein, E., Métois, M., Meneses, G., Vigny, C., and Delorme, A. Bridging the gap between North and Central Chile: insight from new GPS data on coupling complexities and the Andean sliver motion. *Geophysical Journal International*, 213(3):1924–1933, Mar. 2018. doi: 10.1093/gji/ggy094.
- Laske, G., Masters, G., Ma, Z., and Pasyanos, M. Update on CRUST1.0 — A 1-degree global model of Earth's crust. In *Geophysical research abstracts*, volume 15, page 2658, 2013.
- Li, S. and Freymueller, J. T. Spatial Variation of Slip Behavior Beneath the Alaska Peninsula Along Alaska-Aleutian Subduction Zone. *Geophysical Research Letters*, 45(8):3453–3460, Apr. 2018. doi: 10.1002/2017gl076761.
- Li, S., Moreno, M., Bedford, J., Rosenau, M., and Oncken, O. Revisiting viscoelastic effects on interseismic deformation and locking degree: A case study of the Peru-North Chile subduction zone. *Journal of Geophysical Research: Solid Earth*, 120(6), 2015. doi: 10.1002/2015jb011903.
- Li, S., Wang, K., Wang, Y., Jiang, Y., and Dosso, S. E. Geodetically Inferred Locking State of the Cascadia Megathrust Based on a Viscoelastic Earth Model. *Journal of Geophysical Research: Solid Earth*, 123(9), 2018. doi: 10.1029/2018jb015620.
- Lindsey, E. O., Mallick, R., Hubbard, J. A., Bradley, K. E., Almeida, R. V., Moore, J. D. P., Bürgmann, R., and Hill, E. M. Slip rate deficit and earthquake potential on shallow megathrusts. *Nature Geoscience*, 14(5):321–326, May 2021. doi: 10.1038/s41561-021-00736-x.
- Lindsey, E. O., Wang, Y., Aung, L. T., Chong, J.-H., Qiu, Q., Mallick, R., Feng, L., Aung, P. S., Tin, T. Z. H., Min, S. M., Bradley, K., Than, O., Oo, K. M., Thant, M., Masson, F., Bürgmann, R., and Hill, E. M. Active subduction and strain partitioning in western Myanmar revealed by a dense survey GNSS network. *Earth and Planetary Science Letters*, 622:118384, Nov. 2023. doi: 10.1016/j.epsl.2023.118384.
- Liu, Z., Owen, S., Dong, D., Lundgren, P., Webb, F., Hetland, E., and Simons, M. Estimation of interplate coupling in the Nankai trough, Japan using GPS data from 1996 to 2006. *Geophysical Journal International*, Apr. 2010. doi: 10.1111/j.1365-246x.2010.04600.x.
- Loveless, J. P. and Meade, B. J. Two decades of spatiotemporal variations in subduction zone coupling offshore Japan. *Earth and Planetary Science Letters*, 436:19–30, Feb. 2016. doi: 10.1016/j.epsl.2015.12.033.
- Loverly, B., Chlieh, M., Norabuena, E., Villegas-Lanza, J. C., Radiguet, M., Cotte, N., Tsapong-Tsague, A., Quiroz, W., Sierra Farfán, C., Simons, M., Nocquet, J. M., Tavera, H., and Socquet, A. Heterogeneous Locking and Earthquake Potential on the South Peru Megathrust From Dense GNSS Network. *Journal of Geophysical Research: Solid Earth*, 129(2), Jan. 2024. doi: 10.1029/2023jb027114.
- Loverly, B., Radiguet, M., Chlieh, M., Norabuena, E., Villegas-Lanza, J. C., Cresseaux, J., Ragon, T., Tsapong-Tsague, A., Tavera, H., and Socquet, A. Viscoelastic Relaxation Following the 2001 $M_w=8.4$ Arequipa Earthquake and Its Impact on the Interseismic Coupling of the South Peru Megathrust. *Geophysical Research Letters*, 52(12), 2025. doi: 10.1029/2024gl113879.
- Luo, H., Wang, K., Feng, L., and Hill, E. M. Interseismic secondary zone of subsidence during earthquake cycles in subduction zones. *Nature Geoscience*, 18(10):1027–1033, Aug. 2025. doi: 10.1038/s41561-025-01778-1.
- Mai, P. M. and Thingbaijam, K. K. S. SRCMOD: An Online Database of Finite-Fault Rupture Models. *Seismological Research Letters*, 85(6):1348–1357, Oct. 2014. doi: 10.1785/0220140077.
- Mai, P. M., Schorlemmer, D., Page, M., Ampuero, J., Asano, K., Causse, M., Custodio, S., Fan, W., Festa, G., Galis, M., Gallovic, F., Imperatori, W., Käser, M., Malysky, D., Okuwaki, R., Pollitz, F., Passone, L., Razafindrakoto, H. N. T., Sekiguchi, H., Song, S. G., Somala, S. N., Thingbaijam, K. K. S., Twardzik, C., van Driel, M., Vyas, J. C., Wang, R., Yagi, Y., and Zielke, O. The Earthquake-Source Inversion Validation (SIV) Project. *Seismological Research Letters*, 87(3):690–708, Apr. 2016a. doi: 10.1785/0220150231.

- Mai, P. M., Shearer, P., Ampuero, J., and Lay, T. Standards for Documenting Finite-Fault Earthquake Rupture Models. *Seismological Research Letters*, 87(3):712–718, Apr. 2016b. doi: 10.1785/0220150204.
- Materna, K., Murray, J. R., Pollitz, F., and Patton, J. R. Slip Deficit Rates on Southern Cascadia Faults Resolved with Viscoelastic Earthquake Cycle Modeling of Geodetic Deformation. *Bulletin of the Seismological Society of America*, 113(6), 2023. doi: 10.1785/0120230007.
- Maubant, L., Radiguet, M., Pathier, E., Doin, M.-P., Cotte, N., Kazachkina, E., and Kostoglodov, V. Interseismic coupling along the Mexican subduction zone seen by InSAR and GNSS. *Earth and Planetary Science Letters*, 586:117534, May 2022. doi: 10.1016/j.epsl.2022.117534.
- Maubant, L., Frank, W. B., Wallace, L. M., Williams, C. A., and Hamling, I. Imaging the Spatiotemporal Evolution of Plate Coupling With Interferometric Radar (InSAR) in the Hikurangi Subduction Zone. *Geophysical Research Letters*, 50(19), Oct. 2023. doi: 10.1029/2023gl105388.
- Meade, B. J. Algorithms for the calculation of exact displacements, strains, and stresses for triangular dislocation elements in a uniform elastic half space. *Computers & Geosciences*, 33(8): 1064–1075, Aug. 2007. doi: 10.1016/j.cageo.2006.12.003.
- Melgar, D. Was the January 26th, 1700 Cascadia Earthquake Part of a Rupture Sequence? *Journal of Geophysical Research: Solid Earth*, 126(10), Oct. 2021. doi: 10.1029/2021jb021822.
- Melnick, D., Bookhagen, B., Strecker, M. R., and Echtler, H. P. Segmentation of megathrust rupture zones from fore-arc deformation patterns over hundreds to millions of years, Arauco peninsula, Chile. *Journal of Geophysical Research: Solid Earth*, 114 (B1), Jan. 2009. doi: 10.1029/2008jb005788.
- Michel, S., Gualandi, A., and Avouac, J.-P. Interseismic Coupling and Slow Slip Events on the Cascadia Megathrust. *Pure and Applied Geophysics*, 176(9), 2018. doi: 10.1007/s00024-018-1991-x.
- Michel, S., Jolivet, R., Klein, E., and Maubant, L. 14 Years of Slip on the Hikurangi Subduction Zone. *Journal of Geophysical Research: Solid Earth*, 130(7), 2025. doi: 10.1029/2024jb030865.
- Minson, S. E., Simons, M., and Beck, J. L. Bayesian inversion for finite fault earthquake source models I—theory and algorithm. *Geophysical Journal International*, 194(3), 2013. doi: 10.1093/gji/ggt180.
- Moreno, M. S., Bolte, J., Klotz, J., and Melnick, D. Impact of megathrust geometry on inversion of coseismic slip from geodetic data: Application to the 1960 Chile earthquake. *Geophysical Research Letters*, 36(16), Aug. 2009. doi: 10.1029/2009gl039276.
- Métois, M., Socquet, A., and Vigny, C. Interseismic coupling, segmentation and mechanical behavior of the central Chile subduction zone. *Journal of Geophysical Research: Solid Earth*, 117 (B3), Mar. 2012. doi: 10.1029/2011jb008736.
- Métois, M., Socquet, A., Vigny, C., Carrizo, D., Peyrat, S., Delorme, A., Maureira, E., Valderas-Bermejo, M.-C., and Ortega, I. Revisiting the North Chile seismic gap segmentation using GPS-derived interseismic coupling. *Geophysical Journal International*, 194(3), 2013. doi: 10.1093/gji/ggt183.
- Métois, M., Vigny, C., and Socquet, A. Interseismic Coupling, Megathrust Earthquakes and Seismic Swarms Along the Chilean Subduction Zone (38°–18°S). *Pure and Applied Geophysics*, 173 (5):1431–1449, Apr. 2016. doi: 10.1007/s00024-016-1280-5.
- Nishimura, T., Yokota, Y., Tadokoro, K., and Ochi, T. Strain partitioning and interplate coupling along the northern margin of the Philippine Sea plate, estimated from Global Navigation Satellite System and Global Positioning System-Acoustic data. *Geosphere*, 14(2):535–551, Feb. 2018. doi: 10.1130/ges01529.1.
- Noda, A., Saito, T., and Fukuyama, E. Slip-Deficit Rate Distribution Along the Nankai Trough, Southwest Japan, With Elastic Lithosphere and Viscoelastic Asthenosphere. *Journal of Geophysical Research: Solid Earth*, 123(9), 2018. doi: 10.1029/2018jb015515.
- Okada, Y. Surface deformation due to shear and tensile faults in a half-space. *International Journal of Rock Mechanics and Mining Sciences & Geomechanics Abstracts*, 23(4):128, Aug. 1986. doi: 10.1016/0148-9062(86)90674-1.
- Okada, Y. Internal deformation due to shear and tensile faults in a half-space. *Bulletin of the Seismological Society of America*, 82 (2):1018–1040, Apr. 1992. doi: 10.1785/bssa0820021018.
- Oryan, B. Code for the coupling cloud, Dec. 2025. doi: 10.5281/zenodo.17821569.
- Oryan, B. and Gabriel, A.-A. Do Coupled Megathrusts Rupture? *EarthArXiv*, 2025. doi: 10.31223/X5HB3N.
- Panda, D. and Lindsey, E. O. Overriding Plate Deformation Controls Inferences of Interseismic Coupling Along the Himalayan Megathrust. *Journal of Geophysical Research: Solid Earth*, 129 (9), 2024. doi: 10.1029/2024jb029819.
- Perry, M., Muller, C., Protti, M., Feng, L., and Hill, E. M. Interseismic Megathrust Coupling at the Osa Peninsula, Costa Rica. *Journal of Geophysical Research: Solid Earth*, 130(7), 2025. doi: 10.1029/2024jb030641.
- Philibosian, B. and Meltzner, A. J. Segmentation and supercycles: A catalog of earthquake rupture patterns from the Sumatran Sunda Megathrust and other well-studied faults worldwide. *Quaternary Science Reviews*, 241:106390, Aug. 2020. doi: 10.1016/j.quascirev.2020.106390.
- Plata-Martinez, R., Iinuma, T., Tomita, F., Nakamura, Y., Nishimura, T., and Hori, T. Revisiting Slip Deficit Rates and Its Insights Into Large and Slow Earthquakes at the Nankai Subduction Zone. *Journal of Geophysical Research: Solid Earth*, 129(12), Dec. 2024. doi: 10.1029/2023jb027942.
- Pollitz, F. F. Gravitational viscoelastic postseismic relaxation on a layered spherical Earth. *Journal of Geophysical Research: Solid Earth*, 102(B8):17921–17941, Aug. 1997. doi: 10.1029/97jb01277.
- Pollitz, F. F. 3D Viscoelastic Models of Slip-Deficit Rate Along the Cascadia Subduction Zone. *Journal of Geophysical Research: Solid Earth*, 130(1), Jan. 2025. doi: 10.1029/2024jb029847.
- Pollitz, F. F. and Evans, E. L. Implications of the earthquake cycle for inferring fault locking on the Cascadia megathrust. *Geophysical Journal International*, page ggx009, Jan. 2017. doi: 10.1093/gji/ggx009.
- Radiguet, M., Perfettini, H., Cotte, N., Gualandi, A., Valette, B., Kostoglodov, V., Lhomme, T., Walpersdorf, A., Cabral Cano, E., and Campillo, M. Triggering of the 2014 Mw7.3 Papanao earthquake by a slow slip event in Guerrero, Mexico. *Nature Geoscience*, 9 (11):829–833, Oct. 2016. doi: 10.1038/ngeo2817.
- Ramos, M. D., Huang, Y., Ulrich, T., Li, D., Gabriel, A., and Thomas, A. M. Assessing Margin-Wide Rupture Behaviors Along the Cascadia Megathrust With 3-D Dynamic Rupture Simulations. *Journal of Geophysical Research: Solid Earth*, 126(7), 2021. doi: 10.1029/2021jb022005.
- Rew, R. and Davis, G. NetCDF: an interface for scientific data access. *IEEE Computer Graphics and Applications*, 10(4), 1990. doi: 10.1109/38.56302.
- Rousset, B., Lasserre, C., Cubas, N., Graham, S., Radiguet, M., DeMets, C., Socquet, A., Campillo, M., Kostoglodov, V., Cabral-Cano, E., Cotte, N., and Walpersdorf, A. Lateral Variations of Interplate Coupling along the Mexican Subduction Interface: Relationships with Long-Term Morphology and Fault Zone Mechanical Properties. *Pure and Applied Geophysics*, 173(10-11):

- 3467–3486, Dec. 2015. doi: 10.1007/s00024-015-1215-6.
- Savage, J. C. A dislocation model of strain accumulation and release at a subduction zone. *Journal of Geophysical Research: Solid Earth*, 88(B6), 1983. doi: 10.1029/jb088ib06p04984.
- Schlömer, N. meshio: Tools for mesh files, Mar. 2022. doi: 10.5281/zenodo.6346837.
- Schmalzle, G. M., McCaffrey, R., and Creager, K. C. Central Cascadia subduction zone creep. *Geochemistry, Geophysics, Geosystems*, 15(4):1515–1532, Apr. 2014. doi: 10.1002/2013gc005172.
- Schroeder, W., Martin, K. W., Martin, K., and Lorensen, B. *The Visualization Toolkit*. Prentice Hall, Old Tappan, NJ, 2nd edition, 1998.
- Scott, D. W. On optimal and data-based histograms. *Biometrika*, 66(3):605–610, 12 1979. doi: 10.1093/biomet/66.3.605.
- Sherrill, E. M., Johnson, K. M., and Jackson, N. M. Locating Boundaries Between Locked and Creeping Regions at Nankai and Cascadia Subduction Zones. *Journal of Geophysical Research: Solid Earth*, 129(10), Oct. 2024. doi: 10.1029/2024jb029346.
- Small, D. T. and Melgar, D. Geodetic Coupling Models as Constraints on Stochastic Earthquake Ruptures: An Example Application to PTHA in Cascadia. *Journal of Geophysical Research: Solid Earth*, 126(7), 2021. doi: 10.1029/2020jb021149.
- Stevens, V. L. and Avouac, J. P. Interseismic coupling on the main Himalayan thrust. *Geophysical Research Letters*, 42(14), 2015. doi: 10.1002/2015gl064845.
- Sullivan, C. and Kaszynski, A. PyVista: 3D plotting and mesh analysis through a streamlined interface for the Visualization Toolkit (VTK). *Journal of Open Source Software*, 4(37):1450, May 2019. doi: 10.21105/joss.01450.
- Tarantola, A. *Inverse Problem Theory and Methods for Model Parameter Estimation*. Society for Industrial and Applied Mathematics, Jan. 2005. doi: 10.1137/1.9780898717921.
- Tarantola, A. and Valette, B. Generalized nonlinear inverse problems solved using the least squares criterion. *Reviews of Geophysics*, 20(2):219–232, May 1982. doi: 10.1029/rg020i002p00219.
- Tomita, F., Iinuma, T., Agata, R., and Hori, T. Development of a Trans-Dimensional Fault Slip Inversion for Geodetic Data. *Journal of Geophysical Research: Solid Earth*, 126(5), May 2021. doi: 10.1029/2020jb020991.
- Tsang, L. L. H., Meltzner, A. J., Hill, E. M., Freymueller, J. T., and Sieh, K. A paleogeodetic record of variable interseismic rates and megathrust coupling at Simeulue Island, Sumatra. *Geophysical Research Letters*, 42(24), Dec. 2015. doi: 10.1002/2015gl066366.
- van Rijsingen, E., Calais, E., Jolivet, R., de Chabalière, J., Jara, J., Smithe, S., Robertson, R., and Ryan, G. Inferring Interseismic Coupling along the Lesser Antilles Arc: a Bayesian Approach. 2020. doi: 10.31223/osf.io/kn7hq.
- Villegas-Lanza, J. C., Chlieh, M., Cavalié, O., Tavera, H., Baby, P., Chire-Chira, J., and Nocquet, J. Active tectonics of Peru: Heterogeneous interseismic coupling along the Nazca megathrust, rigid motion of the Peruvian Sliver, and Subandean shortening accommodation. *Journal of Geophysical Research: Solid Earth*, 121(10):7371–7394, Oct. 2016. doi: 10.1002/2016jb013080.
- Wallace, L. M., Barnes, P., Beavan, J., Van Dissen, R., Litchfield, N., Mountjoy, J., Langridge, R., Lamarche, G., and Pondard, N. The kinematics of a transition from subduction to strike-slip: An example from the central New Zealand plate boundary. *Journal of Geophysical Research: Solid Earth*, 117(B2), Feb. 2012. doi: 10.1029/2011jb008640.
- Wang, K. and Dixon, T. “Coupling” Semantics and science in earthquake research. *Eos, Transactions American Geophysical Union*, 85(18):180–180, May 2004. doi: 10.1029/2004eo180005.
- Wang, K., Hu, Y., and He, J. Deformation cycles of subduction earthquakes in a viscoelastic Earth. *Nature*, 484(7394):327–332, Apr. 2012. doi: 10.1038/nature11032.
- Wang, K., Zhu, Y., Nissen, E., and Shen, Z. On the Relevance of Geodetic Deformation Rates to Earthquake Potential. *Geophysical Research Letters*, 48(11), 2021. doi: 10.1029/2021gl093231.
- Wang, L., Hainzl, S., and Mai, P. M. Quantifying slip balance in the earthquake cycle: Coseismic slip model constrained by interseismic coupling. *Journal of Geophysical Research: Solid Earth*, 120(12):8383–8403, Dec. 2015. doi: 10.1002/2015jb011987.
- Wang, Z. Seismic Hazard Assessment: Issues and Alternatives. *Pure and Applied Geophysics*, 168(1-2):11–25, May 2010. doi: 10.1007/s00024-010-0148-3.
- Wessel, P., Luis, J. F., Uieda, L., Scharroo, R., Wobbe, F., Smith, W. H. F., and Tian, D. The Generic Mapping Tools Version 6. *Geochemistry, Geophysics, Geosystems*, 20(11):5556–5564, Nov. 2019. doi: 10.1029/2019gc008515.
- Widiyantoro, S., Gunawan, E., Muhari, A., Rawlinson, N., Mori, J., Hanifa, N. R., Susilo, S., Supendi, P., Shiddiqi, H. A., Nugraha, A. D., and Putra, H. E. Implications for megathrust earthquakes and tsunamis from seismic gaps south of Java Indonesia. *Scientific Reports*, 10(1), 2020. doi: 10.1038/s41598-020-72142-z.
- Wilkinson, M. D., Dumontier, M., Aalbersberg, I. J., Appleton, G., Axton, M., Baak, A., Blomberg, N., Boiten, J.-W., da Silva Santos, L. B., Bourne, P. E., Bouwman, J., Brookes, A. J., Clark, T., Crosas, M., Dillo, I., Dumon, O., Edmunds, S., Evelo, C. T., Finkers, R., Gonzalez-Beltran, A., Gray, A. J., Groth, P., Goble, C., Grethe, J. S., Heringa, J., ‘t Hoen, P. A., Hooft, R., Kuhn, T., Kok, R., Kok, J., Lusher, S. J., Martone, M. E., Mons, A., Packer, A. L., Persson, B., Rocca-Serra, P., Roos, M., van Schaik, R., Sansone, S.-A., Schultes, E., Sengstag, T., Slater, T., Strawn, G., Swertz, M. A., Thompson, M., van der Lei, J., van Mulligen, E., Velterop, J., Waagmeester, A., Wittenburg, P., Wolstencroft, K., Zhao, J., and Mons, B. The FAIR Guiding Principles for scientific data management and stewardship. *Scientific Data*, 3(1), Mar. 2016. doi: 10.1038/sdata.2016.18.
- Xue, L., Schwartz, S., Liu, Z., and Feng, L. Interseismic megathrust coupling beneath the Nicoya Peninsula, Costa Rica, from the joint inversion of InSAR and GPS data. *Journal of Geophysical Research: Solid Earth*, 120(5):3707–3722, May 2015. doi: 10.1002/2014jb011844.
- Yabuki, T. and Matsu’ura, M. Geodetic data inversion using a Bayesian information criterion for spatial distribution of fault slip. *Geophysical Journal International*, 109(2):363–375, May 1992. doi: 10.1111/j.1365-246x.1992.tb00102.x.
- Yokota, Y., Ishikawa, T., Watanabe, S.-i., Tashiro, T., and Asada, A. Seafloor geodetic constraints on interplate coupling of the Nankai Trough megathrust zone. *Nature*, 534(7607):374–377, May 2016. doi: 10.1038/nature17632.

The article *The Coupling Cloud: A community database of megathrust kinematic coupling models* © 2026 by Bar Oryan is licensed under CC BY 4.0.